catalysts

MDPI

Article

Novel Complex Titanium NASICON-Type Phosphates as Acidic Catalysts for Ethanol Dehydration

Anna I. Zhukova [1], Elena A. Asabina [2], Andrey N. Kharlanov [3], Diana A. Osaulenko [1], Sofia G. Chuklina [1], Dmitry Yu. Zhukov [4], Vladimir I. Pet'kov [2] and Dina V. Deyneko [3,5,*]

1 Department of Physical and Colloid Chemistry, Peoples Friendship University of Russia (RUDN University), 6, Miklukho-Maklaya Str., Moscow 117198, Russia
2 Department of Chemistry, Lobachevsky University, Nizhny Novgorod 603950, Russia
3 Department of Chemistry, Lomonosov Moscow State University, Moscow 119991, Russia
4 Technology Centre, Mendeleev University of Chemical Technology, 9, Miusskaya Squ., Moscow 125047, Russia
5 Laboratory of Arctic Mineralogy and Material Sciences, Kola Science Centre, Russian Academy of Sciences, 14 Fersman Str., Apatity 184209, Russia
* Correspondence: deynekomsu@gmail.com

Abstract: The conversion of ethanol towards ethylene and diethyl ether in the presence of catalysts requires special consideration from the perspective of green chemistry. Ethanol dehydration was studied on a complex titanium phosphate MAlTiP ($M_{0.5(1+x)}Al_xTi_{2-x}(PO_4)_3$ with M = Ni, Mn (x = 0; 0.2)) catalysts, alongside a NASICON-type structure synthesized by the sol–gel method. The initial catalysts were characterized by N_2 gas sorption, SEM, XRD and spectroscopic methods (Raman and DRIFT of adsorbed CO and C_6H_6). The results revealed that all catalysts exhibited high activity and selectivity at 300–420 °C. The conversion of ethanol increases with the reaction temperature, reaching 67–80% at 420 °C. The MnAlTiP exhibited the highest ethylene selectivity among other catalysts, with 87% at 420 °C. The aluminum modification improved the acid properties of the catalysts, due to the appearance of Lewis acid sites (LAS) and the strength moderate Brønsted acid sites (BAS). It was shown that the activity of complex phosphates in ethanol dehydration increases with the strength of the Brønsted acid sites (BAS).

Keywords: complex titanium phosphates; NASICON; ethanol dehydration; ethylene; diethyl ether; Lewis acid sites; Brønsted acid sites

Citation: Zhukova, A.I.; Asabina, E.A.; Kharlanov, A.N.; Osaulenko, D.A.; Chuklina, S.G.; Zhukov, D.Y.; Pet'kov, V.I.; Deyneko, D.V. Novel Complex Titanium NASICON-Type Phosphates as Acidic Catalysts for Ethanol Dehydration. *Catalysts* **2023**, *13*, 185. https://doi.org/10.3390/catal13010185

Academic Editors: Oleg Vladislavovich Levin, Daniil A. Lukyanov and Elena Alekseeva

Received: 2 December 2022
Revised: 9 January 2023
Accepted: 9 January 2023
Published: 13 January 2023

1. Introduction

Recently, the development of new environmentally friendly and efficient catalysts for the dehydration process, in order to synthesize value-added chemicals from biomass-based substrates, has become desirable [1]. From this point of view, NASICON-type (sodium (Na-) super ionic conductor) materials, which possess a regular phosphate structure with abundant acidic and basic sites on the surface, correspond to the specified properties. For the typical NASICON-type material, octahedron and tetrahedron units are interlinked via corner-share oxygen atoms to construct the basic unit of the structure [2,3]. The distinctive features of this material are a high cation conductivity, good thermostability, well-developed pores, and the presence of abundant oxygen-containing species or hydroxyl groups on the surface. It is worth noting their high chemical stability and structure variability, which make it possible to carry out both iso- and heterovalent doping, without destroying the original cavity of the NASICON structure [4]. The propensity for heterovalent substitution is particularly important for their use as catalysts in acid-base reactions; this allows them to vary the number and the strength of acid sites on the surface, which determines the selectivity of the target and by-product formation in catalytic reactions [5–8].

With all the variety of reactions occurring on complex phosphates, the chemistry of ethanol is of interest; this is due to its potential use as a highly efficient chemical bio-based

platform that can be converted into targeted chemical compounds [1,9,10]. Furthermore, the conversion of alcohols is also used as a test reaction for surface acidity–basicity characterization [11,12]. Recently, the NASICON catalysts' activity in the conversion of light alcohols (such as butanol, ethanol and methanol) has been studied [6,13–17]. The product distribution was very different depending on the phosphate's composition. It has been shown that Li-Zr- and Hf-phosphates are promising catalysts for the production of hydrocarbons from ethanol [18–20].

Several assumptions have been made about the nature of the active centers of NASICON-type complex phosphates in alcohol's dehydration [18–20]. In the case of complex zirconium phosphates, the Brønsted acid sites are OH-groups coordinated with zirconium (Zr–OH, strong Brønsted acid sites) and with phosphorus (P–OH, weak Brønsted acid sites); meanwhile, the Lewis acid sites are incompletely coordinated Zr^{4+} ions [21]. Although the dehydration of alcohols over solid catalysts occurs on mainly acid sites, the strong acidity and non-uniform distribution of these sites leads to undesirable by-products and significant coking [22]. In this regard, an increase in the number of moderately strong or weak acid sites is used for an improvement in the catalysts' dehydration properties [23,24].

More recently, the NASICON-type nickel titanium phosphate ($Ni_{0.5}Ti_2(PO_4)_3$ [25] and hydrogen titanium phosphate sulfate (HTPS; $H_{1-x}Ti_2(PO_4)_{3-x}(SO_4)_x$, x = 0.5–1) [26] showed a high selectivity for the dehydrogenation of methanol to formaldehyde, and also for the conversion of ethanol to acetaldehyde. While good performance was attributed to redox activity (the reducibility of Ti^{4+} to Ti^{3+}), the expected acidity of the titanium phosphate framework structure is worth noting.

In the present study, we report on the use of the NASICON-type double (binary) nickel and manganese–titanium phosphate, triple nickel–aluminum–titanium, and manganese–aluminum–titanium phosphate catalysts MAlTiP ($M_{0.5(1+x)}Al_xTi_{2-x}(PO_4)_3$ with M = Ni, Mn; x = 0; 0.2) for ethanol dehydration. The Ni^{2+} or Mn^{2+} ions are located in the conductivity channels of the structure. The influence of 3*d* cation nature (nickel or magnesium) in the cavity of the NASICON structure, and the substitution of Ti^{4+} by Al^{3+} in the framework on the catalytic activity, was investigated. Composition–structure–activity relationships were also studied using various techniques, including X-ray diffraction (XRD), scanning electron microscopy (SEM) and Raman spectroscopy. Special attention was paid to the surface acid properties of the catalysts using a Fourier transform infrared spectroscopy (FTIR) analysis of CO and C_6H_6 adsorption.

The catalysts were denoted as MnTiP ($Mn_{0.5}Ti_2(PO_4)_3$, x = 0), MnAlTiP ($Mn_{0.6}Al_{0.2}Ti_{1.8}(PO_4)_3$, x = 0.2), NiTiP ($Ni_{0.5}Ti_2(PO_4)_3$, x = 0), NiAlTiP ($Ni_{0.6}Al_{0.2}Ti_{1.8}(PO_4)_3$, x = 0.2).

2. Results and Discussion

2.1. X-ray Diffraction Study

Figure 1a shows the XRD patterns of the Mn-containing samples. The reference XRD data for $Mn_{0.5}Ti_2(PO_4)_3$ (MnTiP) [27] are shown in Figure 1b. The NiTiP structure has been previously detailed [25]. According to [27], the diffraction peaks at 2θ = 12–13°, 14.6°, 20.8°, 24.5°, 29.6°, and 33.2° were a characteristic peak of the NASICON phase and were assigned to th e(003), (012), (110), (113), (024), (116) plane orientations. XRD patterns of all single-phase samples are similar in position and intensity to reflections, and indicate that they belong to the structural type $NaZr_2(PO_4)_3$ (space group $R\bar{3}$). The crystal structures of such compounds are based on the framework built up of TiO_6 (or $(Al/Ti)O_6$) and PO_4 polyhedra, while Mn^{2+} or Ni^{2+} ions occupy the cavities within the polyhedra columns. In the MnTiP and NiTiP structures, half the cavities are occupied in an orderly manner [25]. The lattice parameters of the synthesized compounds are presented in Table 1. After the catalytic tests, the structure of the samples remained the same (Figure 1, MnTiP used), but an increase in the amorphous component was observed in the appearance of halos in their XRD patterns. The change in the lattice parameters of the samples after the experiment did not exceed the calculation uncertainty (for example, for MnTiP used: a = 8.517(5) Å, c = 21.02(4) Å).

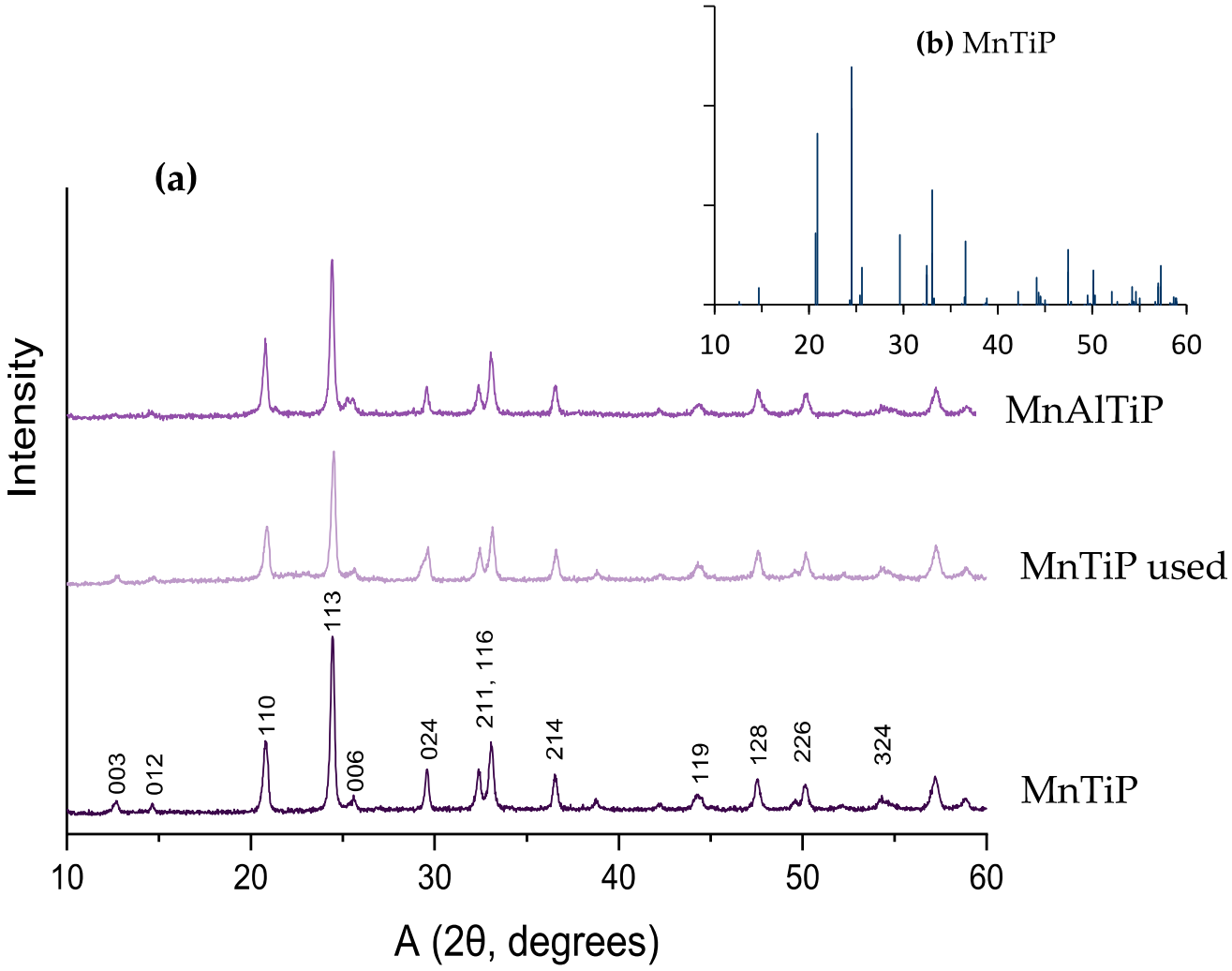

Figure 1. (**a**) XRD patterns of catalysts: $Mn_{0.5}Ti_2(PO_4)_3$ (MnTiP) initial, $Mn_{0.5}Ti_2(PO_4)_3$ used (MnTiP used), $Mn_{0.6}Al_{0.2}Ti_{1.8}(PO_4)_3$ (MnAlTiP) initial; (**b**) XRD data for $Mn_{0.5}Ti_2(PO_4)_3$ (MnTiP) simulated basing on the structural data [27].

Table 1. Lattice parameters of the studied catalysts.

Composition	*a*, Å	*c*, Å
MnTiP	8.515(4)	21.06(2)
MnAlTiP	8.516(5)	21.05(3)
NiTiP	8.478(5)	21.14(4)
NiAlTiP	8.478(1)	20.97(8)

2.2. Raman Spectroscopy

Figure 2 shows the Raman spectra from 2000 to 50 cm^{-1} of catalysts. For the typical NASICON-type structure of the rhombohedral compound, TiO_6 octahedron and PO_4 tetrahedron units are interlinked via corner-share oxygen atoms to construct the basic unit of the structure. The peaks at 940–1100 cm^{-1} in the spectra correspond to the stretching vibrations of phosphate ions in the NASICON-type structure (ν_{as} = 1083, 1050, 1038, 1003 cm^{-1}; ν_s = 976, 939 cm^{-1}). The band at 427 cm^{-1} was ascribed to the symmetric bending vibration of the phosphate structure. Otherwise, the band assigned to the translations and vibration of the PO_4 unit was observed at 344 cm^{-1}. The bands below 300 cm^{-1} were due to TiO_6 internal modes [28–30].

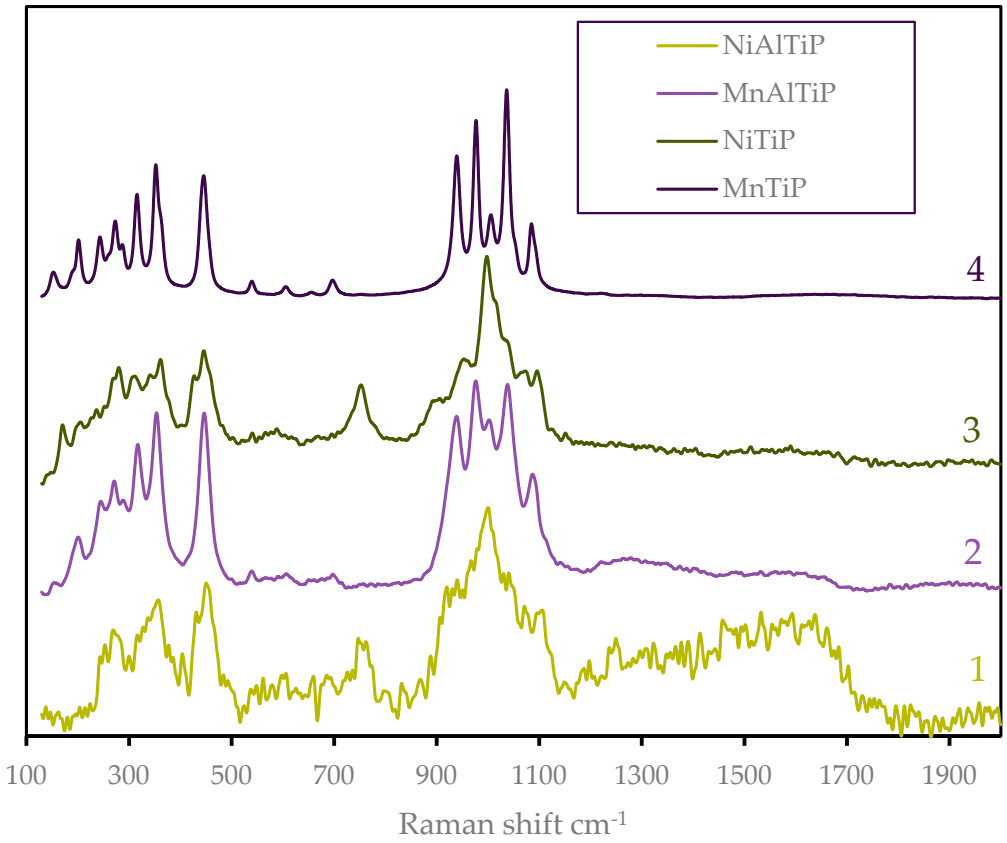

Figure 2. Raman spectra of (1) NiAlTi, (2) MnAlTi, (3) NiTi, (4) MnTi.

Raman scattering is typically sensitive to the degree of crystallinity in the sample; the spectra of crystalline materials show narrow intense peaks, while those of amorphous materials are broader and less intense [31]. The Raman spectra of the Mn-containing samples (Figure 2, lines 2 and 4) show narrow symmetric lines that can be associated with a well-formed phosphate structure. The Raman spectra of the Ni-containing samples (Figure 2, lines 1 and 3) show broad lines. The intensities of the bands for MnAlTiP are higher than those for NiAlTiP. Thus, in the presence of nickel ions, a defective phosphate structure is formed.

We associate the structural features of NiTiP with a small Ni^{2+} radius, relative to the cavities of the NASICON structure; this leads to structural defects and makes the structure unstable. The MnTiP is thermally stable up to 1223 K [3], while the NiTiP is only stable up to 953 K [25].

2.3. Microscopic Morphology and Porosity

Figure 3a,b shows the N_2 sorption isotherms and BJH pore distributions of the samples. The isotherms are a combination of type-III and type-V, with a type H3 hysteresis; this indicates the presence of both mesopores and macropores [32], which is in accordance with data for TiP NASICON-type materials [29]. Double NiTiP shows its hysteresis loop at a much higher p/p_0 position in comparison to the others, indicating that its pore sizes are bigger. This can be seen more clearly in the corresponding BJH pore size distributions in Figure 3b. Samples NiTiP, NiAlTiP and MnAlTiP showed a pore size distribution with a broad maximum between 15 to 27 nm. The broad peak at approximately 20 nm is a common feature of these phosphates. For the MnTiP sample, the peak maximum is shifted to 50 nm, and there is a much broader size distribution. This shift indicates that pore coarsening starts to occur drastically without Al in the MnTiP structure.

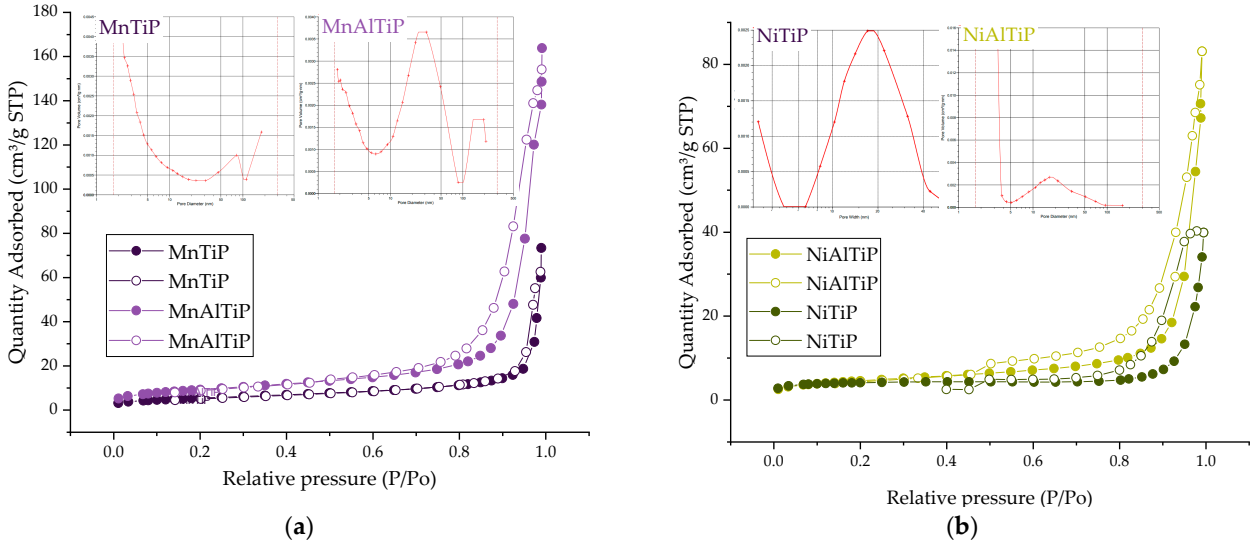

Figure 3. Nitrogen adsorption–desorption isotherms and pore size distributions of the compounds: (**a**) $Mn_{0.5}Ti_2(PO_4)_3$ (MnTiP), $Mn_{0.6}Al_{0.2}Ti_{1.8}(PO_4)_3$ (MnAlTiP) and (**b**) $Ni_{0.5}Ti_2(PO_4)_3$ (NiTiP), $Ni_{0.6}Al_{0.2}Ti_{1.8}(PO_4)_3$ (NiAlTiP).

Table 2 summarizes the pore characteristics. The Brunauer–Emmett–Teller (BET) surface area and the pore volume of MnTiP were higher than the surface area and pore volume of NiTiP; these corresponded to the ionic radius dopants Mn^{2+} (0.80 Å) and Ni^{2+}(0.69 Å). The substitution of Ti^{4+} (0.56 Å) for Al^{3+} (0.53 Å) also induced the textural property changes. The BET surface area of MnAlTiP was more than 1.7 times higher than that of MnTiP (and pore volume was more than 2.3 times higher), due to the doping of alumina that is more prone to mesopore formation. In the case of the Ni-containing samples, the pore volume was much larger for the sample with the Al substitution, as expected. However, the other values are not as significantly different for double and triple Ni-containing phosphates.

Table 2. BET surface area and porous characteristics of the compounds $M_{0.5(1+x)}Al_xTi_{2-x}(PO_4)_3$.

Composition	BET Surface (m^2/g)	Pore Volume (cm^3/g)	Average Pore Diameter (nm)
MnTiP	20.0	0.11	23
MnAlTiP	33.6	0.25	23
NiTiP	13.6	0.06	17
NiAlTiP	16.6	0.13	20

The scanning electron microscope (SEM) images in Figure 4 show that the surface of the catalysts is rough, covered with smaller spheric-shaped or coral-shaped particles. Higher magnification SEM images in Figure 4b,d,f,h reveal that these aggregated particles have a nanostructured surface texture. Figure 4b,f shows SEM micrographs of the MnTiP and NiTiP samples, which exhibit nanoparticles that are strongly fused together to form textural pores less than approximately 200 nm. A subtle difference in the surface textures can be seen in Figure 4h, showing fewer aggregated surface particles in the NiAlTiP sample.

2.4. Diffuse Reflectance Infrared Fourier Transform Spectroscopy (DRIFT) Study of Adsorbed CO and C_6H_6

Carbon monoxide is widely used as a probe molecule to detect the presence and the nature of Lewis acidic sites [33–35]. The spectral changes obtained by adsorption of different CO pressures on $M_{0.5(1+x)}Al_xTi_{2-x}(PO_4)_3$ are represented in Figure 5a,b.

The FTIR spectrum of CO adsorption on NiAlTiP is the superposition of absorption bands (AB) at 2202–2204, 2184 and 2130–2133 cm^{-1} (Figure 5a). The bands at 2202–2204 and 2184 cm^{-1} can be attributed to carbonyl species, adsorbed on Ni^{2+} cations [36] and

associated with carbonyl complexes with the strength-moderate LAS (Lewis acid sites). The band at 2130 cm^{-1} can be attributed to CO adsorbed on $Ni^{\delta+}$ sites ($\delta < 1$) [36]. Note that a change in the CO pressure had an effect on the view of the NiAlTiP spectrum; at 5 Torr (Figure 5a, black line), there is no line at 2130 cm^{-1}. With the increase in the CO pressure from 5 to 25 Torr, the intensity of the peak at 2184 cm^{-1} decreased. At the same time, the peak at 2130–2133 cm^{-1} appeared (Figure 5a, red and blue lines). On the one hand, this allows us to interpret the absorption band at 2184 cm^{-1} as contributing to CO complexes with Ni^{2+}. On the other hand, this fact indicates the possibility of reducing Ni^{2+} in the CO atmosphere.

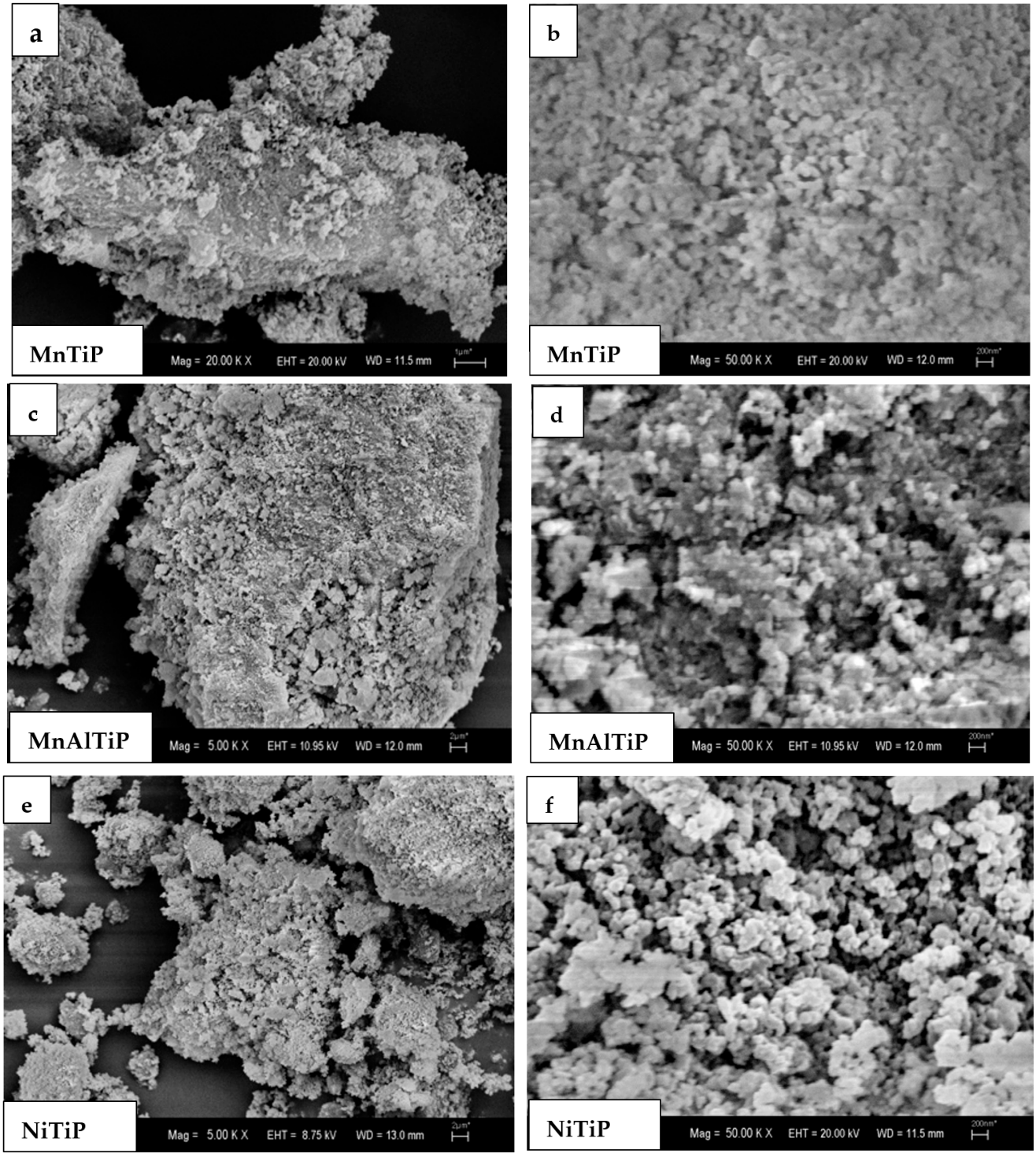

Figure 4. *Cont.*

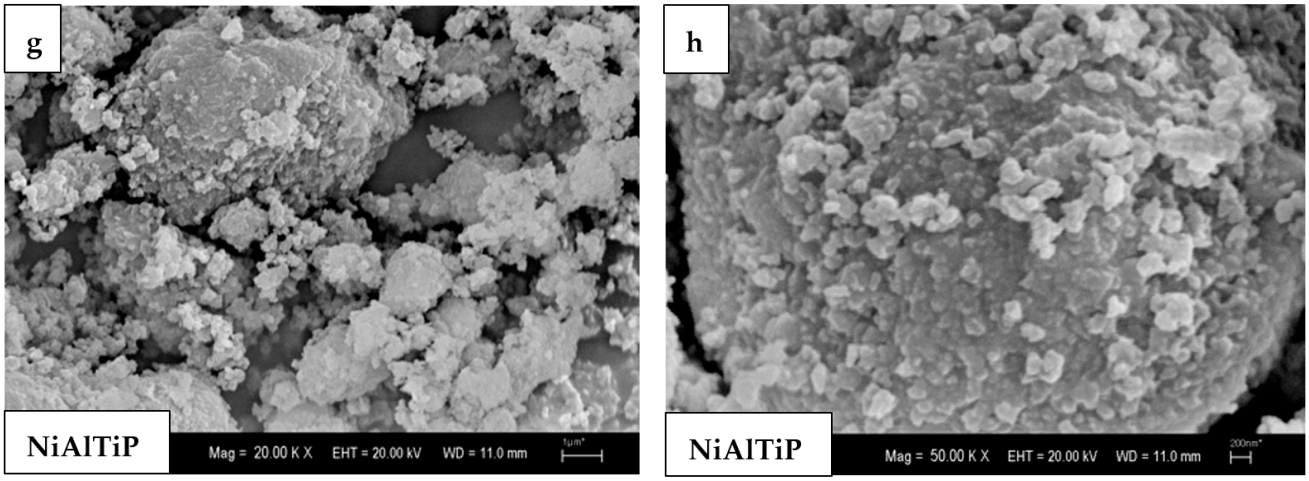

Figure 4. Scanning electron microscopy of $Mn_{0.5}Ti_2(PO_4)_3$ (MnTiP), $Mn_{0.6}Al_{0.2}Ti_{1.8}(PO_4)_3$ (MnAlTiP), $Ni_{0.5}Ti_2(PO_4)_3$ (NiTiP), $Ni_{0.6}Al_{0.2}Ti_{1.8}(PO_4)_3$ (NiAlTiP).

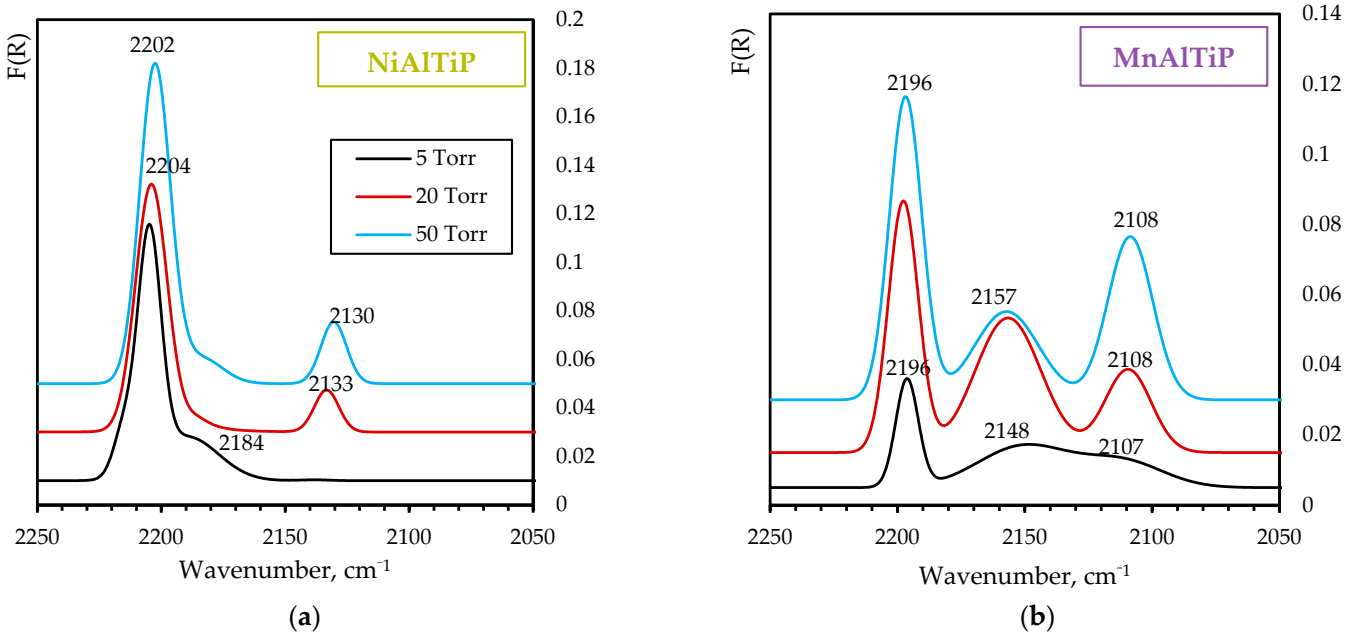

Figure 5. Different diffuse reflectance infrared Fourier transform spectra of adsorbed CO at room temperature and pressure (1) 5 Torr, (2) 20 Torr, (3) 50 Torr. F(R)—Kubelka–Munk function.

The FTIR spectrum of CO adsorption on MnAlTiP at 5 Torr contains the superposition of three absorption bands with wavenumbers at 2196, 2148–2157 and 2108–2109 cm^{-1} (Figure 5b). According to the classification of carbonyl complex bands [36], these absorption bands can be attributed to CO adsorbed on Mn^{2+}, $Mn^{\delta+}$ cations ($\delta < 1$) and metallic Mn^0. The same intensity in the peaks can mean that a significant number of Mn^{2+} cations reduced to $Mn^{\delta+}$ or Mn^0. In addition, with the increase in CO pressure, $Mn^{\delta+}$ further reduces to a metal state. The relative intensity of the absorption band at 2148–2157 cm^{-1} decreases, and the absorption band at 2108–2109 cm^{-1} increases (Figure 5b, red and blue lines).

Note that, with the increase in the CO pressure, the band intensity of absorbed CO rises due to an increase in the degree of filling in the LAS by CO molecules. Simultaneously, the CO molecules may displace other adsorbed molecules or hydroxyl groups. The significant increase in the band intensity at 2196 cm^{-1} in Figure 5b is due to the displacement of part of the OH-groups from LAS. For the Ni-containing system, such a process does not play a significant role (Figure 5a, band intensity at 2022 cm^{-1}).

The adsorption of CO does not produce carbonyl complexes on the surface of binary NiTiP and MnTiP systems. This can be explained by the inaccessibility of Ni and Mn cations during surface reconstruction under thermal vacuum treatment conditions.

The phosphates possess the three types of OH-groups that correspond to the absorption bands at 3743–3745, 3697–3711 and 3663–3678 cm^{-1} [37]. These bands can be attributed to the Brønsted acid sites (BASs). The strength of BASs was characterized by proton affinity (*PA*), that is, the energy of proton detachment from the surface OH group during the formation of a hydrogen bond with benzene molecules [38]. The data obtained are shown in Table 3. In accordance with [39], we can estimate the *PA* value for OH-groups. For terminal hydroxyl groups (3743–3745 cm^{-1}), the shift is 143–148 cm^{-1}, which corresponds to weak proton donor properties. For bridging hydroxyl groups (3663–3678 cm^{-1}), the highest shift was $\Delta\nu$ = 190 cm^{-1} on the MnAlTiP surface, and the smallest shift was $\Delta\nu$ = 162 cm^{-1} on the MnTi surface. On the NiTiP and NiAlTiP systems, the shifts were $\Delta\nu$ = 178 and $\Delta\nu$ = 171 cm^{-1}, respectively. Thus, aluminum promotes an increase in proton affinity, especially on Mn-containing systems. These shifts correspond to medium-strength Bronsted centers (on all systems). For hydroxyl groups at 3697–3711 cm^{-1}, it was not possible to determine proton donor properties due to the low intensity of the band.

Table 3. Acidic characteristics of the catalysts.

Composition	ν(OH), cm^{-1}	ν(OH ... C_6H_6), cm^{-1}	$\Delta\nu$, cm^{-1}	*PA*, kJ/mol ± 25
NiAlTiP	3745	3602	143	1340
	3678	3500	178	1230
MnAlTiP	3745	3601	144	1340
	3711	-	-	-
	3677	3487	190	1285
NiTiP	3743	3595	148	1335
	3697	-	-	
	3663	3492	171	1305
MnTiP	3744	3601	143	1340
	3698	-	-	-
	3667	3505	162	1315

2.5. Catalytic Tests in Ethanol Conversion

The NASICON-type catalysts $M_{0.5(1+x)}Al_xTi_{2-x}(PO_4)_3$, with different Mn(Ni)/Ti/Al/P ratios, were used for the ethanol conversion in the vapor-phase, as a model reaction, proceeding in three main ways: dehydration to form ethylene or/and diethyl ether (DEE) and dehydrogenization to form acetaldehyde (AcH). The reaction was carried out at 280–420 °C.

All synthesized compounds showed high activity in the alcohol conversion. The conversion of ethanol (Figure 6) increases with the reaction temperature, reaching 67–80% at 420 °C. Doping MeTiP with Al^{3+} increases the ethanol conversion by ~20%, which is consistent with an increase in the specific surface area. There was no deactivation under the reaction flow. The total conversion was the same for triple Al-containing phosphates, and increased for double phosphates (without Al) in repeated experiments (Figure 6, open square). The results obtained in this study confirm those already observed with other dehydration catalysts, namely, that pore sizes of 10 nm or more are needed to slow down the deactivation attributed to the irreversible adsorption of oligomer species and/or to the formation of coke (Table 2, Figure 3).

In the case of the ethanol-to-hydrocarbon process, the mechanism of acid-catalyzed ethanol dehydration assumed the production of ethylene via the direct conversion of ethanol (Equation (1)). At low temperatures (>340 °C), DEE is generated in significant quantities (Equation (2)), but at high temperatures (<380 °C), ethylene becomes a dominant

product. Alcohol dehydrogenation, in order to produce AcH (Equation (3)), can also occur as a side reaction at the higher temperatures [40].

$$C_2H_5OH \rightarrow C_2H_4 + H_2O \quad (1)$$

$$2C_2H_5OH \rightarrow C_2H_5OC_2H_5 + H_2O \quad (2)$$

$$C_2H_5OH \rightarrow CH_3CHO + H_2 \quad (3)$$

On all samples, the main products were DEE and ethylene. There was also some AcH as a by-product. The ethanol dehydration, with the formation of DEE at low temperatures, was the dominant process for all catalysts (Figure 6). The selectivity of this process reaches 50–75% on MnTiP and NiAlTiP catalysts at temperatures of approximately 300–340 °C. A significant number of ethylene formation processes take place for all catalysts at elevated temperatures. The results obtained for ethanol dehydration are summarized and compared with other NASICON-type catalysts from the literature in Table 4.

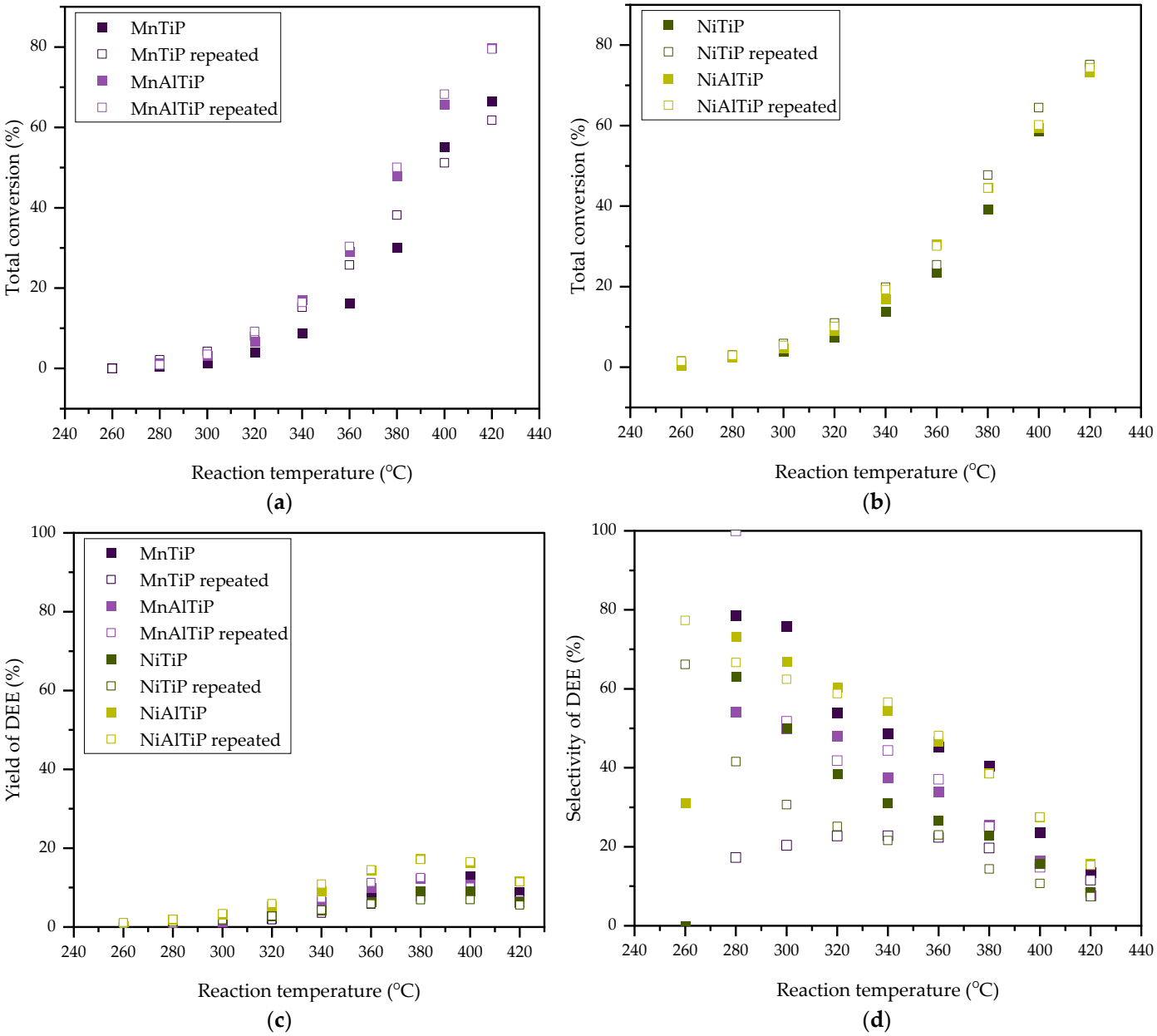

Figure 6. *Cont.*

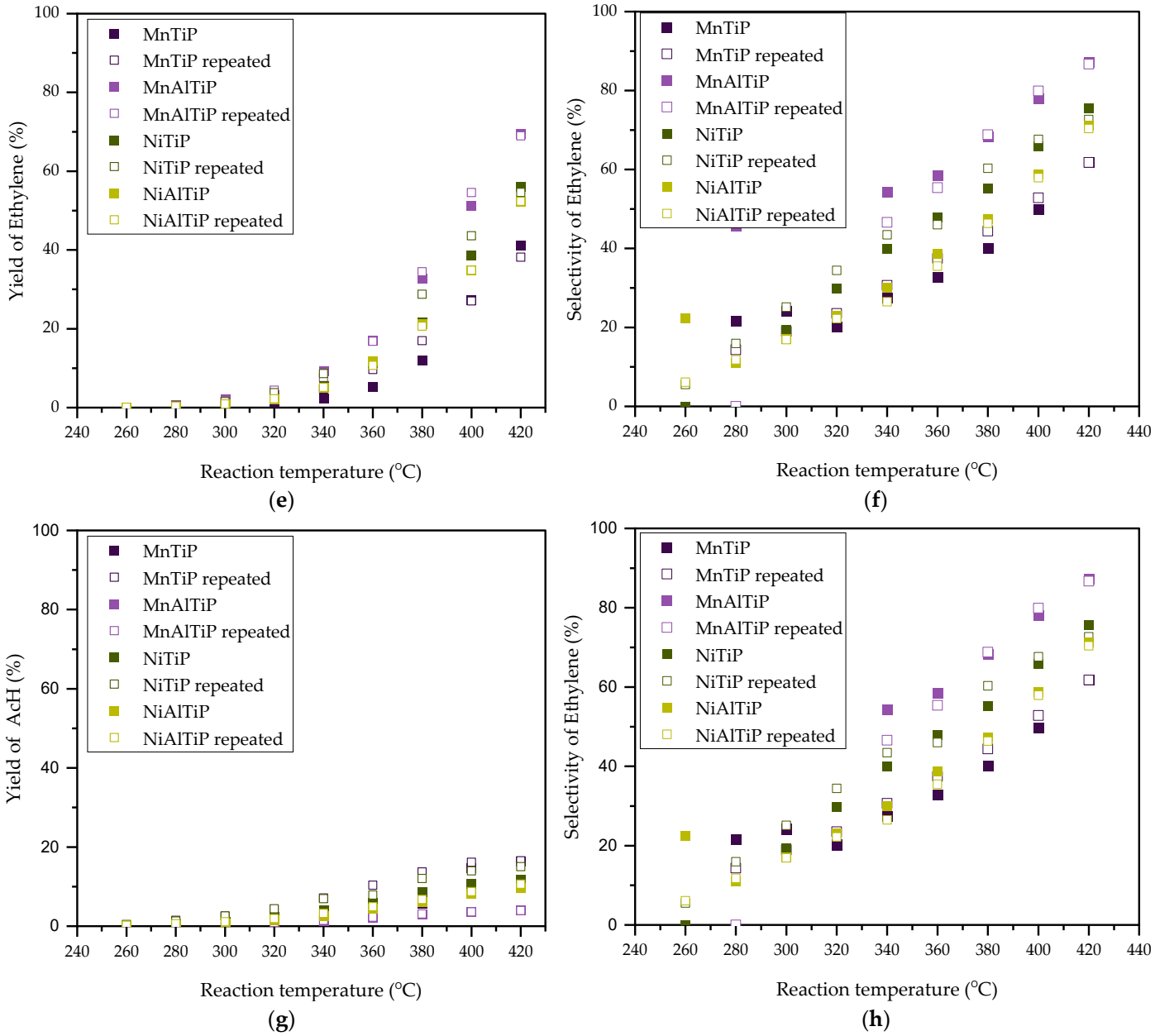

Figure 6. Temperature (°C) dependencies of total ethanol conversion (%) on the initial surface and for repeated test (**a**,**b**); Temperature dependencies of the yield and selectivity of diethyl ether (**c**,**d**), ethylene (**e**,**f**) and acetaldehyde (**g**,**h**). Open squares are used for the repeated experiment.

Table 4. Performance of various catalysts for ethanol dehydration to ethylene at 400 °C.

Composition of the Catalysis	Selectivity to Ethylene (%)	Ethylene Yield (%)	Reference
NiAlTiP	58	34	This work
MnAlTiP	80	51	This work
NiTiP	68	39	This work
MnTiP	50	27	This work
$Mn_{0.5}Zr_2(PO_4)_3$	17	6	[41]
$MnNi_{0.5}Zr_{1.5}(PO_4)_3$	10	4	[41]
$LiHf_2(PO_4)_3$	55	40	[19]

Table 4. *Cont.*

Composition of the Catalysis	Selectivity to Ethylene (%)	Ethylene Yield (%)	Reference
$LiZr_2(PO_4)_3$	38	38	[14]
$Li_{1.1}Hf_{1.9}In_{0.1}(PO_4)_3$	40	32	[19]
HTPS-650	60	55	[26]
$NH_4Hf_2(PO_4)_3$	60	48	[20]

Among the studied phosphates, the MnAlTiP material presented the highest conversion of ethanol and the highest yields of ethylene, providing the Ti–OH groups of the highest strength. On the contrary, the least active and selective material was MnTiP, providing the Ti–OH groups with the least strength (Table 3). In the studied temperature range, the activity of double MnTiP and NiTiP phosphates is close, but the selectivity for the ethylene formation on NiTiP is higher than on MnTiP; it is here that inter-molecular dehydration, with the formation of DEE, predominantly occurs at T < 380 °C.

From the results of this study, the highest value for the frequency shift $\Delta\nu_{OH} \ldots C_6H_6$ was found in the MnAlTi material, and the decrease in the acid strength of the Ti–OH groups follow the following trend: MnAlTiP > NiAlTiP > NiTi > MnTi. It becomes clear that the stronger the BAS, the more active the solid acid is, with respect to the ethylene formation. This tendency becomes more obvious when comparing the values of ethylene yields and depending on the strength of BASs (proton affinity) in the NASICON phosphates. This result is in good accordance with those obtained for other catalysts for the ethanol dehydration [42,43].

It is noteworthy that the heterovalent doping effect is most clearly manifested in ethanol dehydrogenation. The partial substitution of titanium for aluminum decreases the dehydrogenating properties of the catalyst. Moreover, if the AcH formation predominates, in the case of samples without aluminum (binary phosphates) at low temperatures in the repeat experiments (Figure 6, open squares), the selectivity for dehydrogenation does not change in the triple phosphates and remains low throughout the temperature range. The titanium phosphates are more active than zirconia phosphates in converting ethanol [41], but even less selective to ethylene, mainly due to the higher production of AcH (40% yield at 673 K).

The catalytic activity in the dehydration of ethanol is attributed to the acid properties; these are a function of the Brønsted acid sites, and are incompletely coordinated 3*d* cations that have a strong polarization effect (Lewis acid sites) [21]. In the case of complex phosphates $M_{0.5(1+x)}Al_xTi_{2-x}(PO_4)_3$, the Brønsted acid sites are OH groups coordinated with titanium (medium Brønsted acid sites) and with phosphorus (weak Brønsted acid sites), while the Lewis acid sites are incompletely coordinated Ni^{2+} or Mn^{2+} ions.

Thus, the activity of MAlTiP in ethanol dehydration increases with the strength of the BASs. The difference in the effects of ethanol dehydration (ethylene's or DEE's formation processes) on NiAlTiP or MnAlTiP may be caused by the strength of the LAS, depending on the nature of 3*d* metal in the cavity of the NASICON structure.

3. Materials and Methods

3.1. Synthesis of the Catalysts

The following starting reactants were used for synthesis: $Mn(CH_3COO)_2{\cdot}4H_2O$ (≥99%), $Ni(CH_3COO)_2{\cdot}4H_2O$ (≥99%), $Al(NO_3)_3{\cdot}9H_2O$ (≥99.9%), $TiCl_3$ (15% aqueous solution), $NH_4H_2PO_4$ (≥99.5%), citric acid, and ethylene glycol. Previously, the $TiCl_3$ solution was oxidized with concentrated HCl and HNO_3 solutions in the air to produce a solution of titanium oxychloride $TiOCl_2$. The titanium (IV) concentration in the obtained solution was determined via a gravimetric method, using its conversion into a stable oxide form (TiO_2). Other starting salts were dissolved into a distilled water.

During synthesis, the calculated amount of citric acid was added to the stoichiometric mixture of metal salt solutions (molar ratio metals:citric acid was 1:5) and dissolved during heating. Subsequently, ethylene glycol (1:1 to citric acid) and ammonium dihydrogen phosphate were added to the resulting metal–citrate complex at the same time during mixing, until a homogeneous gel was produced. The resulting gel was dried at temperature stages of T = 90, 130, and 250 °C, until there was a complete removal of water and ethylene glycol. Then, the sample was subjected to sequential dispersion and annealing at 600 °C (Mn-phosphates) or 650 °C (Ni-phosphates) for 48 h at each step.

3.2. Characterization of the Catalysts

The X-ray diffraction (XRD) patterns of the synthesized phosphates were recorded on a Shimadzu XRD-6000 (Kyoto, Japan) diffractometer in CuKα-filtered radiation (λ = 1.54178 Å) at room temperature and with a 2θ angle range of 10–60°. The scanning rate was 1 °/min. The obtained experimental data were compared with the data from the literature for MnTiP and NiTiP, presented in [25,27]. On the basis of the structural similarity of the studied compounds, XRD pattern indexing was performed, and the lattice parameters were calculated.

Low temperature nitrogen physisorption isotherms were recorded on a «TriStar-3020 (Norcross, GA 30093, USA» Surface Area and Porosity Analyzer after the samples were degassed in a vacuum at 200 °C for 5 h. Then, the Brunauer–Emmett–Teller (BET) model was applied to calculate the specific surface area, and the pore-size distribution was calculated using the Barrett–Joyner–Halenda (BJH) model.

Scanning electron microscopy (SEM) images were taken on the EVO-40 scanning electron microscope (Carl Zeiss, Jena, Germany).

The adsorption properties (Lewis acidity) of the samples were measured by diffuse reflectance FTIR spectroscopy with an EQUINOX 55/S instrument (Bruker, Billerica, MA, USA). The powdered sample was placed in a quartz cell with a CaF_2 window and calcined at 550 °C for 1 h on air, and then calcined for 2 h under a vacuum ($p \leq 5 \times 10^5$ Torr). After that, the background spectrum was recorded. To determine the Lewis acidity of the supports, the adsorbed CO spectra were recorded at room temperature and at 5, 20 and 50 Torr pressures. The differential spectra of the adsorbed CO were obtained by subtracting the background spectrum from the experimental spectrum, followed by the correction of the baseline in an OPUS 6.0 software (Bruker, Billerica, MA, USA). High-purity carbon monoxide (>99.9) was further cleaned by passing it through a liquid nitrogen trap and storing it over calcined molecular sieves. The Brønsted acid sites were obtained from the IR spectra by the H-bond method, with benzene as spectral probe. This procedure made it possible to measure the concentration and strength of the Brønsted acid sites (BASs). The strength of the BASs were characterized by proton affinity (*PA*), that is, the energy of proton detachment from the surface OH group, which was calculated in accordance with the procedure described in [44].

Raman spectra were recorded on a Bruker Equinox 55/S instrument (Bruker, Billerica, MA, USA) with an FRA 106/S attachment. The wavelength of the exciting radiation was 1064 nm, the laser power was 200–400 mW, and the spot size was 0.1 mm. The experimental Raman spectra were normalized to the band with a stronger intensity.

3.3. Catalytic Tests

Catalytic experiments were performed at atmospheric pressure in a tubular flow reactor (i.d. 6 mm) using a 0.03 g catalyst and feeding ethanol in argon; it had a total flow rate of 1.2 L/h). The carrier gas (argon) was passed through a bubbler containing ethanol (97%), maintained at a constant temperature (25 °C), in order to obtain the desired partial pressures. The temperature in the experiment was varied stepwise from 260 to 420 °C. The outlet gases were analyzed by a Chromatec-Crystal 5000 (Chromatec, Yoshkar-Ola, Russia) gas chromatograph (GC), equipped with a "Parapak Q" column and TCD and FID

detectors in series. Measurements were performed according to the methodology of our previous studies [41].

4. Conclusions

The high efficiency of NASICON-type phosphates $M_{0.5(1+x)}Al_xTi_{2-x}(PO_4)_3$ with M = Ni^{2+}, Mn^{2+} in the ethanol dehydration process has been shown. All catalysts appeared to be catalytically active and stable in the 300–420 °C temperature range, giving diethyl ether, ethylene and acetaldehyde as the by-products. A similar high activity in ethanol conversion, but different selectivity to ethylene and diethyl ether, were found. The conversion of ethanol increases with the reaction temperature, reaching 67–80% at 420 °C. Considering ethylene production, the MnAlTiP exhibited the highest ethylene selectivity among other catalysts with 87% at 420 °C.

The main aim of the study was to demonstrate the relationship between the composition, the structure of the complex phosphates and its activity in the ethanol dehydration. It has been shown that the crystalline structure and crystallinity of the catalysts varied significantly with different 3*d* metal in the lattice of the NASICON structure. Based on the XRD and Raman spectroscopy data, it was revealed that Mn-containing phosphates had a higher crystallinity than Ni-containing phosphates. It was found that MnTiP has a higher surface area and pore volume than NiTiP, which corresponds to the ionic radius of dopants Mn^{2+} and Ni^{2+}. The substitution of Ti^{4+} for Al^{3+} also induced the textural property changes. The BET surface area of MeAlTiP was higher than that of MeTiP, due to the doping of alumina that is more prone to the mesopore formation (average pore diameter is around 17–23 nm).

The different compositions and chemical environments of the surface elements led to different acid–base properties. Acid properties were studied using an FTIR analysis of CO and C_6H_6 adsorption, and were allowed to be correlated with the catalytic properties. Double MnTiP and NiTiP phosphates have only Brønsted acid sites with broad strength distributions, but they have mainly weak and moderated acid strengths. NiTiP possessed a higher proton affinity than MnTiP. According to the research by K. Zheng [45], phosphates with amorphous structures contributed more to the creation of BAS; this is in good accordance with the obtained results. The aluminum modification improved the acid properties of the catalysts, due to the appearance of LAS and the strength-moderate BAS. From the results of the acid property analysis, the appropriate Brønsted/Lewis acid site ratio of the MnAlTiP catalyst can act synergistically; in this way, the catalyst possesses a high activity in ethanol dehydration. The proton affinity of medium Brønsted acid sites appeared to play the main role in ethanol dehydration.

Author Contributions: Conceptualization, A.I.Z.; methodology, A.I.Z.; validation, A.I.Z., S.G.C., E.A.A. and A.N.K.; formal analysis, D.A.O., S.G.C. and V.I.P.; investigation, E.A.A., D.A.O., D.Y.Z. and A.N.K.; data curation, E.A.A., D.A.O., S.G.C. and V.I.P.; writing—original draft preparation, A.I.Z., E.A.A. and A.N.K.; writing—review and editing, A.I.Z., E.A.A., A.N.K. and D.V.D. All authors have read and agreed to the published version of the manuscript.

Funding: This publication has been supported by the RUDN University Scientific Project Grant System. The study was supported by the Development Program of the Interdisciplinary Scientific and Educational School of Lomonosov Moscow State University's "The future of the planet and global environmental change" and the state assignment of the Chemistry Department of Moscow State University (Agreement No. AAAA-A21-121011590086-0) and the state of the Russian Federation, state registration number 122011300125-2.

Data Availability Statement: Data will be available from the corresponding author upon reasonable request.

Conflicts of Interest: The authors declare no conflict of interest.

References

1. Jamil, F.; Aslam, M.; Al-Muhtaseb, A.H.; Bokhari, A.; Rafiq, S.; Khan, Z.; Inayat, A.; Ahmed, A.; Hossain, S.; Khurram, M.S.; et al. Greener and Sustainable Production of Bioethylene from Bioethanol: Current Status, Opportunities and Perspectives. *Rev. Chem. Eng.* **2022**, *38*, 185–207. [CrossRef]
2. Goodenough, J.B.; Hong, H.Y.; Kafalas, J.A. Fast Na^+-ion Transport in Skeleton Structures. *Mater. Res. Bull.* **1976**, *11*, 77843. [CrossRef]
3. Essehli, R.; El Bali, B.; Benmokhtar, S.; Fejfarová, K.; Dusek, M. Hydrothermal Synthesis, Structural and Physico-Chemical Characterizations of Two Nasicon Phosphates: $M_{0.50}{}^{II}Ti_2(PO_4)_3$ (M = Mn, Co). *Mater. Res. Bull.* **2009**, *44*, 1502–1510. [CrossRef]
4. Anantharamulu, N.; Koteswara Rao, K.; Rambabu, G.; Vijaya Kumar, B.; Radha, V.; Vithal, M. A Wide-Ranging Review on Nasicon Type Materials. *J. Mater. Sci.* **2011**, *46*, 2821–2837. [CrossRef]
5. Sadykov, V.A.; Pavlova, S.N.; Zabolotnaya, G.V.; Chaikina, M.V.; Maksimovskaya, R.I.; Tsybulya, S.V.; Burgina, E.B.; Zaikovskii, V.I.; Litvak, G.S.; Frolova, Y.V.; et al. Scientific Bases for the Synthesis of Highly Dispersed Framework Zirconium Phosphate Catalysts for Paraffin Isomerization and Selective Oxidation. *Kinet. Catal.* **2001**, *42*, 432–441. [CrossRef]
6. Ziyad, M.; Arsalane, S.; Kacimi, M.; Coudurier, G.; Millet, J.M.; Védrine, J.C. Behavior of Silver-Thorium Phosphate $AgTh_2(PO_4)_3$ in Butan-2-Ol Conversion. *Appl. Catal. A Gen.* **1996**, *147*, 363–373. [CrossRef]
7. Yamamoto, K.; Abe, Y. Enhanced Catalytic Activity of Microporous Glass-Ceramics with a Skeleton of NASICON-Type Copper(I) Titanium Phosphate Crystal. *Mater. Res. Bull.* **2000**, *35*, 211–216. [CrossRef]
8. Pylinina, A.I.; Akhmedova, L.S.; Knyazeva, E.I.; Fionov, Y.A.; Sokolova, E.A. Acid Properties of Cesium-Nickel-Zirconium Complex Phosphates: Effect on Isobutanol Dehydration. *Pet. Chem.* **2020**, *60*, 592–596. [CrossRef]
9. Sun, J.; Wang, Y. Recent Advances in Catalytic Conversion of Ethanol to Chemicals. *ACS Catal.* **2014**, *4*, 1078–1090. [CrossRef]
10. Fan, D.; Dai, D.J.; Wu, H.S. Ethylene Formation by Catalytic Dehydration of Ethanol with Industrial Considerations. *Materials* **2013**, *6*, 101–115. [CrossRef]
11. Luts, T.; Katz, A. Chemisorption and Dehydration of Ethanol on Silica: Effect of Temperature on Selectivity. *Top. Catal.* **2012**, *55*, 84–92. [CrossRef]
12. Müller, J.M.; Mesquita, G.C.; Franco, S.M.; Borges, L.D.; De Macedo, J.L.; Dias, J.A.; Dias, S.C.L. *Solid-State Dealumination of Zeolites for Use As Catalysts in Alcohol Dehydration*; Elsevier Inc.: Amsterdam, The Netherlands, 2015; Volume 204, ISBN 5561310739.
13. Glukhova, I.O.; Asabina, E.A.; Pet'kov, V.I.; Mironova, E.Y.; Zhilyaeva, N.A.; Kovalskii, A.M.; Yaroslavtsev, A.B. Zirconium D-Transition Metal Phosphates As Catalysts for Selective Dehydration of Methanol to Dimethyl Ether. *Inorg. Mater.* **2020**, *56*, 395–401. [CrossRef]
14. Ilin, A.B.; Orekhova, N.V.; Ermilova, M.M.; Yaroslavtsev, A.B. Catalytic Activity of $LiZr_2(PO_4)_3$ Nasicon-Type Phosphates in Ethanol Conversion Process in Conventional and Membrane Reactors. *Catal. Today* **2016**, *268*, 29–36. [CrossRef]
15. Ilin, A.B.; Ermilova, M.M.; Orekhova, N.V.; Cretin, M.; Yaroslavtsev, A.B. Conversion of Aliphatic C1–C2 Alcohols on In– Nb–Mo-Doped Complex Lithium Phosphates and $HZr_2(PO_4)_3$ with NASICON-Type Structure. *J. Alloys Compd.* **2018**, *748*, 583–590. [CrossRef]
16. Pylinina, A.I.; Mikhalenko, I.I. Catalytic Activity of Thermally Treated $Li_3Fe_2(PO_4)_3$ in the Conversion of Butan-1-Ol. *Mendeleev Commun.* **2012**, *22*, 150–151. [CrossRef]
17. Povarova, E.I.; Pylinina, A.I.; Mikhalenko, I.I. Catalytic Dehydrogenation of Propanol-2 on Na-Zr Phosphates Containing Cu, Co, and Ni. *Russ. J. Phys. Chem. A* **2012**, *86*, 935–941. [CrossRef]
18. Ermilova, M.M.; Sukhanov, M.V.; Borisov, R.S.; Orekhova, N.V.; Pet'Kov, V.I.; Novikova, S.A.; Il'In, A.B.; Yaroslavtsev, A.B. Synthesis of the New Framework Phosphates and Their Catalytic Activity in Ethanol Conversion into Hydrocarbons. *Catal. Today* **2012**, *193*, 37–41. [CrossRef]
19. Novikova, S.A.; Il'in, A.B.; Zhilyaeva, N.A.; Yaroslavtsev, A.B. Catalytic Activity of $Li_{1+X}Hf_{2-X}In_x(PO_4)_3$-Based NASICON-Type Materials for Ethanol Conversion Reactions. *Inorg. Mater.* **2018**, *54*, 676–682. [CrossRef]
20. Moshareva, M.A.; Il'in, A.B.; Zhilyaeva, N.A.; Novikova, S.A.; Yaroslavtsev, A.B. Catalytic Activity of Materials Based on Complex Hafnium Phosphates with the NASICON Structure in Ethanol Conversion. *Nanotechnologies Russ.* **2017**, *12*, 514–519. [CrossRef]
21. Ziyad, M.; Rouimi, M.; Portefaix, J. Activity in Hydrotreatment Processes of Ni-Mo Loaded Zirconium Phosphate $Zr_3(PO_4)_4$. *Appl. Catal. A: Gen.* **1999**, *183*, 93–105. [CrossRef]
22. Nguyen, T.T.N.; Ruaux, V.; Massin, L.; Lorentz, C.; Afanasiev, P.; Maugé, F.; Bellière-Baca, V.; Rey, P.; Millet, J.M.M. Synthesis, Characterization and Study of Lanthanum Phosphates as Light Alcohols Dehydration Catalysts. *Appl. Catal. B Environ.* **2015**, *166–167*, 432–444. [CrossRef]
23. Zhang, X.; Wang, R.; Yang, X.; Zhang, F. Comparison of Four Catalysts in the Catalytic Dehydration of Ethanol to Ethylene. *Microporous Mesoporous Mater.* **2008**, *116*, 210–215. [CrossRef]
24. Zhan, N.; Hu, Y.; Li, H.; Yu, D.; Han, Y.; Huang, H. Lanthanum-Phosphorous Modified HZSM-5 Catalysts in Dehydration of Ethanol to Ethylene: A Comparative Analysis. *Catal. Commun.* **2010**, *11*, 633–637. [CrossRef]
25. Asabina, E.A.; Glukhova, I.O.; Pet'kov, V.I.; Borovikova, E.Y.; Koval'skii, A.M. Synthesis and Structure of Phosphates $M_{0.5}Ti_2(PO_4)_3$. *Russ. J. Gen. Chem.* **2017**, *87*, 684–689. [CrossRef]
26. Mitran, G.; Mieritz, D.G.; Seo, D.K. Highly Selective Solid Acid Catalyst $H_{1-X}Ti_2(PO_4)_{3-x}(SO_4)_x$ for Non-Oxidative Dehydrogenation of Methanol and Ethanol. *Catalysts* **2017**, *7*, 95. [CrossRef]

27. Aatiq, A.; Ménétrier, M.; El Jazouli, A.; Delmas, C. Structural and Lithium Intercalation Studies of $Mn_{(0.5-x)}Ca_xTi_2(PO_4)_3$ Phases ($0 \leq x \leq 0.50$). *Solid State Ion.* **2002**, *150*, 391–405. [CrossRef]
28. Junaid Bushiri, M.; Antony, C.J.; Aatiq, A. Raman and FTIR Studies of the Structural Aspects of Nasicon-Type Crystals; $AFeTi(PO_4)_3$ [A = Ca, Cd]. *J. Phys. Chem. Solids* **2008**, *69*, 1985–1989. [CrossRef]
29. Mieritz, D.; Davidowski, S.K.; Seo, D.K. Accessing Alkali-Free NASICON-Type Compounds through Mixed Oxoanion Sol–Gel Chemistry: Hydrogen Titanium Phosphate Sulfate, $H_{1-x}Ti_2(PO_4)_{3-x}(SO_4)_x$ (X = 0.5–1). *J. Solid State Chem.* **2016**, *242*, 116–125. [CrossRef]
30. Chimie, L.D.; Idriss, B.; Harti, E.; Casablanca, S.O.B.P. Vibrational Spectra and Factor Group Analysis of $Li_{2x}Mn_{0.5-X}Ti_2(PO_4)_3$ {x = 0, 0.25, 0.50}. *Mater. Res.* **1998**, *33*, 955–961.
31. Golubina, E.V.; Kaplin, I.Y.; Maslakov, K.I.; Gorodnova, A.V.; Lokteva, E.S.; Isaikina, O.Y. Non-Oxidative Propane Dehydrogenation on CrO_x-ZrO_2-SiO_2 Catalyst Prepared by One-Pot Template-Assisted Method. *Molecules* **2022**, *27*, 6095. [CrossRef]
32. Alothman, Z.A. A Review: Fundamental Aspects of Silicate Mesoporous Materials. *Materials* **2012**, *5*, 2874–2902. [CrossRef]
33. Manzoli, M. Boosting the Characterization of Heterogeneous Catalysts for H_2O_2 Direct Synthesis by Infrared Spectroscopy. *Catalysts* **2019**, *9*, 30. [CrossRef]
34. Bonelli, B.; Cozzolino, M.; Tesser, R.; Di Serio, M.; Piumetti, M.; Garrone, E.; Santacesaria, E. Study of the Surface Acidity of TiO_2/SiO_2 Catalysts by Means of FTIR Measurements of CO and NH_3 Adsorption. *J. Catal.* **2007**, *246*, 293–300. [CrossRef]
35. Pekounov, Y.; Chakarova, K.; Hadjiivanov, K. Surface Acidity of Calcium Phosphate and Calcium Hydroxyapatite: FTIR Spectroscopic Study of Low-Temperature CO Adsorption. *Mater. Sci. Eng. C* **2009**, *29*, 1178–1181. [CrossRef]
36. Davydov, A. *Molecular Spectroscopy of Oxide Catalyst Surfaces*; Wiley: Chichester, UK, 2003; Volume 33, ISBN 047198731X.
37. Liu, Y.; Chen, Y.; Tian, Y.; Sakthivel, T.; Liu, H.; Guo, S.; Zeng, H.; Dai, Z. Synergizing Hydrogen Spillover and Deprotonation by Internal Polarization Field in a $MoS_2/NiPS_3$ Vertical Heterostructure for Boosted Water Electrolysis. *Adv. Mat.* **2022**, *34*, 2203615. [CrossRef] [PubMed]
38. Paukshtis, E.A.; Kotsarenko, N.S.; Karakchiev, L. G Investigation of Proton—Acceptor Properties of Oxide Surfaces by IR Spectroscopy of Hydrogen-Bonded Complexes. *React. Kinet. Catal. Lett.* **1979**, *12*, 315–319. [CrossRef]
39. Paukshtis, E.A. IR Spectroscopy for Heterogeneous Acid–Base Catalysis, Nauka, Novosibirsk, 1992. In *Studies in Surface Science and Catalysis*; Elsevier: Amsterdam, The Netherlands, 1992. (In Russian)
40. Phillips, C.B.; Datta, R. Production of Ethylene from Hydrous Ethanol on H-ZSM-5 under Mild Conditions. *Ind. Eng. Chem. Res.* **1997**, *36*, 4466–4475. [CrossRef]
41. Mayorov, P.; Asabina, E.; Zhukova, A.; Osaulenko, D.; Pet'kov, V.; Lavrenov, D.; Kovalskii, A.; Fionov, A. Catalytic Properties of the Framework-Structured Zirconium-Containing Phosphates in Ethanol Conversion. *Res. Chem. Intermed.* **2021**, *47*, 3645–3659. [CrossRef]
42. Chaichana, E.; Boonsinvarothai, N.; Chitpong, N.; Jongsomjit, B. Catalytic Dehydration of Ethanol to Ethylene and Diethyl Ether over Alumina Catalysts Containing Different Phases with Boron Modification. *J. Porous Mater.* **2019**, *26*, 599–610. [CrossRef]
43. Takahara, I.; Saito, M.; Inaba, M.; Murata, K. Dehydration of Ethanol into Ethylene over Solid Acid Catalysts. *Catal. Lett.* **2005**, *105*, 249–252. [CrossRef]
44. Badmaev, S.D.; Smorygina, A.S.; Paukshtis, E.A.; Belyaev, V.D.; Sobyanin, V.A.; Parmon, V.N. Gas-Phase Carbonylation of Dimethoxymethane to Methyl Methoxyacetate on Solid Acids: The Effect of Acidity on the Catalytic Activity. *Kinet. Catal.* **2018**, *59*, 99–103. [CrossRef]
45. Zheng, K.; Gao, Q.; Li, C.; Zhang, C.; Wu, Y.; Zhang, Q.; Wang, X.; Zhang, J.; Han, Y.; Tan, Y. A novel and environmentally friendly NASICON-type material: Efficient catalyst for condensation of formaldehyde and acetic acid to acrylic acid and methyl acrylate. *Chem. Ing. J.* **2022**, *446*, 137324. [CrossRef]